Available online at www.sciencedirect.com

ScienceDirect

Journal of Magnesium and Alloys 8 (2020) 345–351

www.elsevier.com/locate/jma

Full Length Article

Microstructure and corrosion resistance of a Mg_2Sn-dispersed Mg alloy subjected to pulsed electron beam treatment

Daseul Lee[a,1], Beomcheol Kim[a,1], Soo-Min Baek[a,1], Jisoo Kim[b], Hyung Wook Park[b], Jung Gu Lee[c], Sung Soo Park[a,*]

[a] School of Materials Science and Engineering, Ulsan National Institute of Science and Technology, Ulsan 44919, Republic of Korea
[b] School of Mechanical, Aerospace and Nuclear Engineering, Ulsan National Institute of Science and Technology, Ulsan 44919, Republic of Korea
[c] School of Materials Science and Engineering, University of Ulsan, Ulsan 44610, Republic of Korea

Received 28 August 2019; received in revised form 6 January 2020; accepted 12 February 2020
Available online 5 May 2020

Abstract

We report that the corrosion resistance of a Mg–Sn-based alloy with Mg_2Sn precipitates can be considerably improved by surface modification using pulsed electron beam treatment. The alloy subjected to a pulse electron beam treatment showed a modified surface layer with a thickness of ~12 μm, appearing more resistant to corrosion attack than the bare surface of the alloy. In 0.6 M NaCl solution, the alloys with and without the surface modification exhibited average corrosion rates of 4.3 and 8.1 mm y^{-1}, respectively. The improved corrosion resistance was attributed to reduced cathodic activation, resulting from the surficial reduction of relatively noble Mg_2Sn precipitates.

Keywords: Magnesium alloy; Mg_2Sn; Intermetallic compound; Pulsed electron beam treatment; Corrosion.

1. Introduction

Mg alloys, the lightest structural alloys, have strong potential for enhancing the fuel efficiency of automobiles as well as the portability of carry-on electronic devices. Unfortunately, however, commercially available Mg–Al- and Mg–Zn-based alloys have inferior mechanical properties compared to competing lightweight materials such as Al alloys, making their use in industrial applications rather sluggish [1]. Recently, extensive efforts to improve the strength and formability levels of Mg alloys by compositional modifications toward the incorporation of Sn, Ca, or a variety of rare-earth elements have been made [2–12].

In particular, Mg–Sn-based alloys have recently drawn substantial interest due to their potential for improving the creep resistance and age hardening capacity of Mg alloys [13–17]. Furthermore, they have been shown to have advantages over conventional Mg alloys when subjected to high-temperature processing such as hot-extrusion and hot-forging [18,19]. These unique properties observable in Mg–Sn-based alloys can be ascribed to the presence of Mg_2Sn precipitates formed in the alloy system. However, recent reports have indicated that Mg–Sn-based alloys have inferior corrosion resistance to conventional Mg alloys [20–24] and their corrosion resistance is worsened as the content of the alloyed Sn increases [21]. This is also closely related to the presence of the Mg_2Sn phase, which is electrochemically nobler than the α-Mg matrix, and thus it can act as cathodic sites that accelerate corrosion in a corrosive condition [21,25].

In the present study, we explored the feasibility of pulsed electron beam (PEB) treatment in selectively eliminating the pre-existing surficial Mg_2Sn precipitates of the Mg–Sn-based alloy to improve its corrosion resistance without substantially sacrificing its original mechanical properties. As a surface modification method, PEB treatment is known to be advantageous over pulsed laser beam and pulsed ion beam treatments

* Corresponding author.
E-mail address: sspark@unist.ac.kr (S.S. Park).
[1] The authors contributed equally to this work.

https://doi.org/10.1016/j.jma.2020.02.005

Table 1
Analyzed chemical composition (wt.%) of the TZAM8110 alloy used in this study.

Alloy	Sn	Zn	Al	Mn	Fe	Si	Ca	Mg
TZAM8110	7.86	0.94	0.82	0.12	0.002	0.003	0.005	bal.

in terms of processing efficiency, simplicity, and reliability [26–28] and its beneficial effects on mechanical properties and corrosion resistance have been reported for some metallic materials [26–32]. For instance, Zhang et al. showed that the hardness and corrosion resistance of pure Ti can be significantly improved by PEB treatment owing to microstructural refinement and enhanced passivation on the surface [29]. Gao et al. reported that commercial AZ91 Mg alloy can have better wear and corrosion resistance due to the surficial formation of an Al-supersaturated solid solution when subjected to PEB treatment [26]. However, few endeavors using PEB treatment to improve the mechanical properties or corrosion resistance of the versatile Mg–Sn-based alloys have been reported to date.

In this study, an experimental Mg–8Sn–1Zn–1Al–0.1Mn (TZAM8110) alloy in an extruded condition was subjected to PEB treatment and the microstructure, tensile properties, and corrosion behavior of the alloys with and without the PEB treatment were comparatively investigated.

2. Experimental procedure

The analyzed composition of the TZAM8110 alloy used in this study is provided in Table 1. A cylindrical billet with the dimensions of an 80 mm diameter and a 150 mm length was used for indirect extrusion executed at a billet temperature of 250 °C and with an extrusion ratio of 25 and a ram speed of 1.3 mm s^{-1}. Prior to the extrusion, the billet was homogenized at 500 °C for 24 h and then water-quenched.

As schematically presented in Fig. 1, the system for the PEB treatment consists of an electron gun, a movable stage, and a vacuum chamber. An electron beam emitted between an anode and a cathode is transmitted in argon gas, generating plasma near the anode. The PEB treatment was performed at an applied voltage of 25 keV, an energy density of 7 J cm^{-2}, a beam diameter of ~60 mm, and an argon gas pressure of 0.05 Pa in the chamber. For microstructural observations and corrosion tests, the PEB treatment was applied on the cross-sections perpendicular to the extrusion direction (ED) and it was repeated 5 times.

Microstructural examinations were performed using a Nikon EPIPHOT 200 optical microscope, a Quanta 200 field-emission scanning electron microscope (SEM), and a JEM-2100F Cs-corrected transmission electron microscope (TEM) equipped with an energy dispersive spectrometer. Samples were basically prepared by grinding with SiC papers up to 1200 grit under a water atmosphere, and they were then polished using a 1 μm diamond paste and a 0.04 μm colloidal silica solution under an ethanol atmosphere. X-ray diffraction (XRD) analysis was performed on the cross-sections perpendicular to the ED using a Bruker D8 ADVANCE in the back reflection mode with Cu Kα radiation. Samples for TEM analysis were prepared using a focused ion beam technique. Tensile tests were conducted at an initial strain rate of 1×10^{-3} s^{-1} using flat tensile specimens with a gage length of 32 mm, a gage width of 5 mm, and a gage thickness of 1.4 mm, respectively. Tensile specimens were machined from the midsections of the extruded alloy and their longitudinal direction is parallel to the ED. To prepare PEB-treated tensile specimens, the PEB treatment was applied on the wide gage section of each specimen 5 times prior to tensile testing.

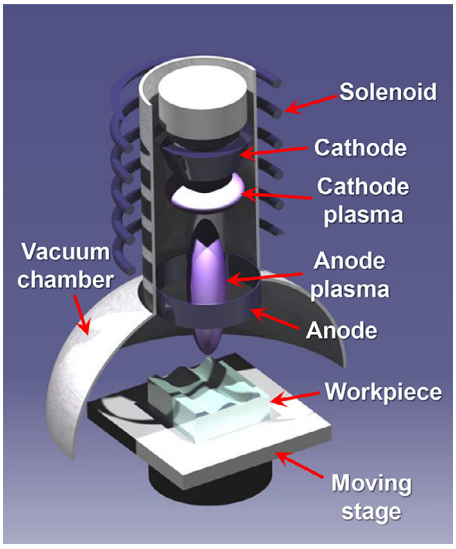

Fig. 1. Three-dimensional schematic diagram of the PEB treatment system.

The corrosion behavior of the as-extruded and PEB-treated samples was investigated using H_2 volume measurements, immersion tests, and potentiodynamic polarization tests in 0.6 M NaCl solution at 25 °C. Cubic samples with a side length of 1.1 mm were used for the H_2 volume measurements and immersion tests. The H_2 volume measurements were performed following a method described in the literature [33]. Depth profiles were obtained using a KEYENCE VHX-6000 optical microscope with the samples cleaned with 200 g l^{-1} CrO_3 solution after immersion in 0.6 M NaCl solution for 12 h. Potentiodynamic polarization tests were done with a GAMRY Reference 600 potentiostat in deaerated 0.6 M NaCl solution at a potential sweep rate of 1 mV s^{-1}. A conventional three-electrode cell comprising a working electrode (sample), a saturated calomel reference electrode (SCE), and a Pt plate counter electrode was used. Each polarization test was done after immersion for 1000 s in the same solution. To ensure the reproducibility, all of the measurements or tests in the present study were performed three times.

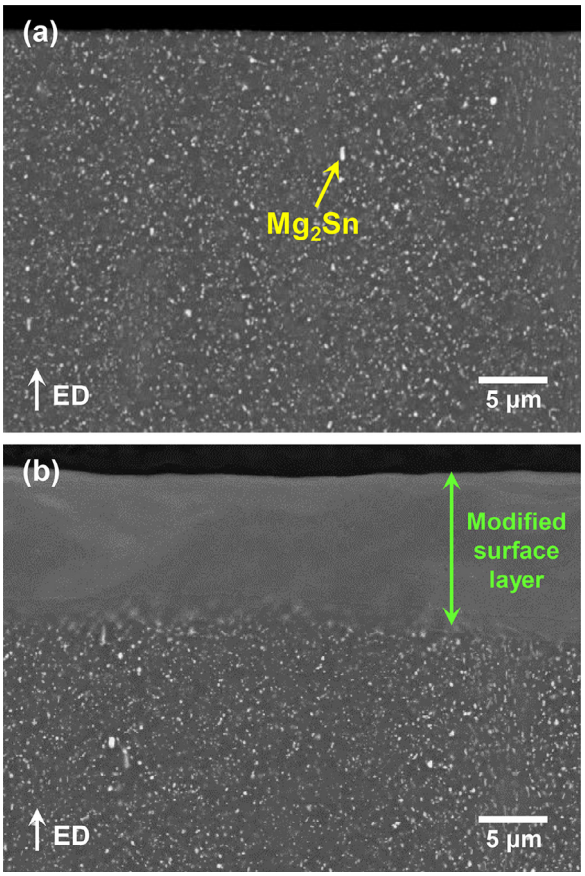

Fig. 2. SEM micrographs showing cross-sections of the (a) as-extruded and (b) PEB-treated samples.

3. Results and discussion

3.1. Microstructure and tensile properties

Figs. 2a and b show SEM micrographs of the as-extruded and PEB-treated samples. The as-extruded sample shows a typical microstructure of Mg–Sn-based alloy extrusions, which contain Mg_2Sn precipitates with sizes of 0.1∼1 μm [23]. Image analysis indicated that the volume fraction of the Mg_2Sn precipitates in the as-extruded sample is ∼3.2%. However, a change in the presence of these precipitates can be seen after the PEB treatment. A modified surface layer with a thickness of ∼12 μm, appearing to be free of the pre-existing Mg_2Sn precipitates, was found in the PEB-treated sample. Also, incipient melting of the pre-existing Mg_2Sn precipitates was not detected anywhere in the modified surface layer, indicating that the pre-existing precipitates were decomposed and then dissolved into the α-Mg matrix without forming a liquid phase during the PEB treatment.

However, the TEM micrographs in Fig. 3 reveal that the modified surface layer of the PEB-treated sample has Mg_2Sn precipitates as well, except for an outmost thin layer with a thickness of ∼250 nm. The Mg_2Sn precipitates in the modified surface layer have an average size of ∼20 nm, which is much smaller than the precipitate sizes of the as-extruded sample without the PEB treatment. The surficial formation of such fine Mg_2Sn precipitate can be attributed to the rapid cooling rate (10^7∼10^8 K s^{-1}) experienced during PEB treatment, as reported elsewhere [29,32]. The average volume fraction of the Mg_2Sn precipitates in the modified surface layer was measured and found to be ∼1.5%. The change in the presence of Mg_2Sn precipitates before and after the PEB treatment is supported by the XRD results in Fig. 4. They show that the diffraction peaks corresponding to the Mg_2Sn phase disappear after the PEB treatment. This is attributed to the presence of the outmost precipitate-free layer as well as the reduced fraction of precipitated particles in the modified surface layer.

Since it has been shown that an electrochemical potential difference between the Mg matrix and secondary phases is a critical factor affecting the corrosion of Mg alloys [34–36], a Volta potential map was acquired by scanning Kelvin probe force microscopy (SKPFM) for the PEB-treated sample, as shown in Fig. 5. Details of the SKPFM measurement are described elsewhere [22,24]. The map demonstrates that Mg_2Sn precipitates appearing in the sample have higher Volta potentials than does the α-Mg matrix, indicating that the intermetallic Mg_2Sn phase has a higher degree of electrochemical nobility than the α-Mg matrix. Correspondingly, it can be seen that the modified surface layer has a Volta potential difference of ∼20 mV at most whereas the region below the surface layer has a relatively higher value of ∼70 mV. This suggests that the PEB-affected surficial layer with reduced Mg_2Sn precipitates would have a lower degree of susceptibility to microgalvanic corrosion than the surface of the as-extruded sample under a corrosive environment.

Fig. 6 shows the tensile stress-strain curves of the as-extruded and PEB-treated samples. It can be seen that the PEB treatment has a marginal effect on deteriorating strength as well as improving ductility. The as-extruded and PEB-treated samples showed tensile yield strengths of 277.1±1.5 and 270.5±1.2 MPa, respectively, and also exhibited tensile elongations of 11.1±0.3 and 11.5±0.4%, respectively. These small differences in tensile properties between the as-extruded and PEB-treated samples are considered to be closely associated with the shallow depth (∼12 μm) of the PEB-affected surface layer.

3.2. Corrosion properties

Figs. 7a-f show the macroscopic changes of the as-extruded and PEB-treated samples during immersion for up to 12 h in 0.6 M NaCl solution. In general, localized corrosion appeared to occur in both samples. After immersion for 0.5 h, severe corrosion pits showing vigorous H_2 evolution formed in the as-extruded sample while the PEB-treated sample appeared to be free of such active pit formation at this point. With prolonged time, the localized corrosion in the as-extruded sample was found to proceed rapidly and thus nearly no metallic luster was retained after immersion for 12 h. On the other hand, the PEB-treated sample showed quite uniform corrosion behavior until immersion up to 0.5 h, followed by relatively sluggish filiform corrosion.

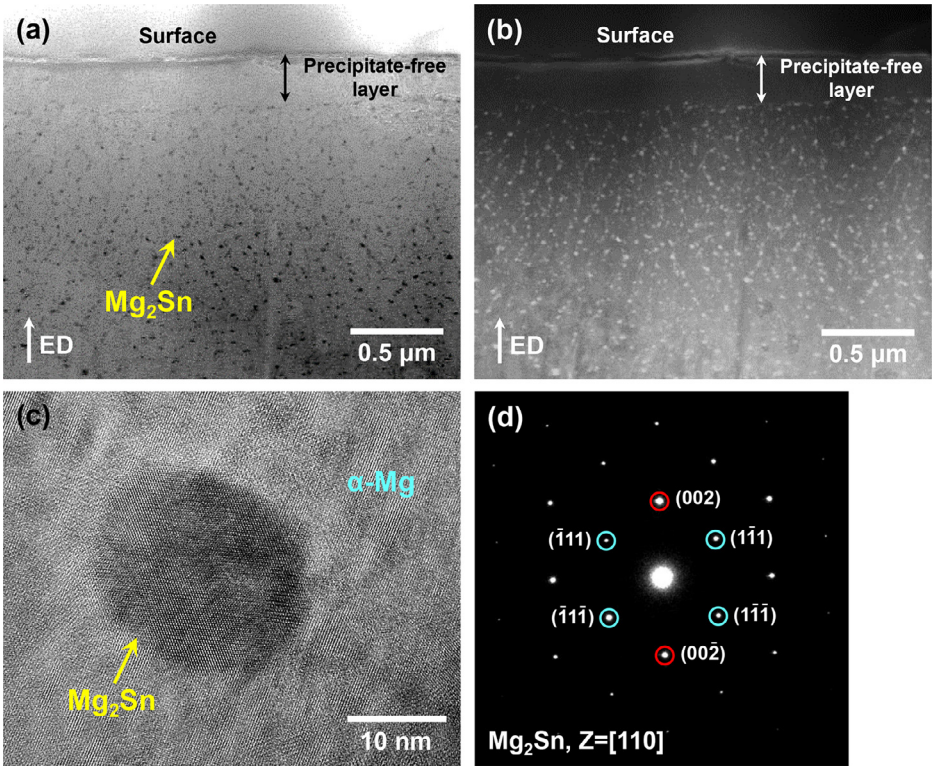

Fig. 3. Low-magnification (a) bright-field and (b) dark-field TEM micrographs showing cross-sections of the modified surface layer in the PEB-treated sample and (c) a high-resolution TEM micrograph showing a Mg_2Sn particle in the modified surface layer with the (d) electron diffraction pattern from the high-resolution TEM micrograph.

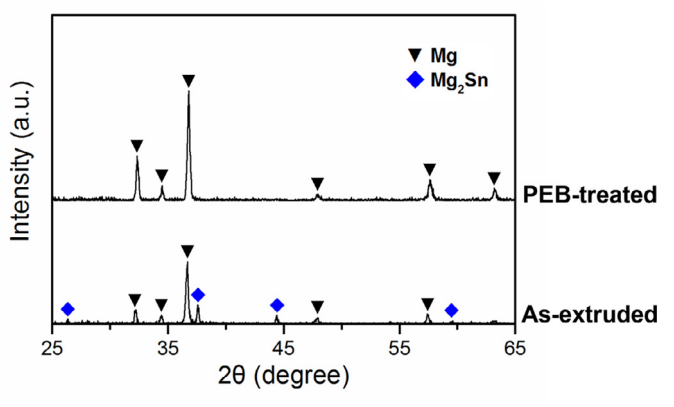

Fig. 4. XRD analysis results of the as-extruded and PEB-treated samples.

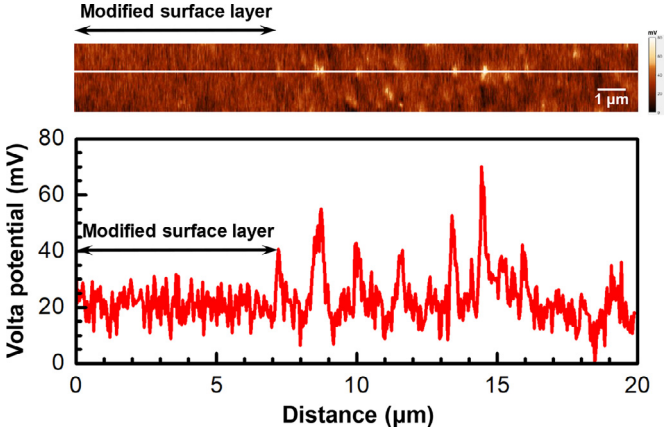

Fig. 5. SKPFM image of the PEB-treated sample and corresponding Volta potential profile along the white line in the image.

After immersion for 12 h, the PEB-treated sample showed corrosion depths of less than ~15 μm without severe surface degradation while the as-extruded sample showed relatively large depths approaching ~80 μm at severely corroded regions, as indicated in Figs. 7g and h. This comparison of the macroscopic changes in the corrosive environment clearly shows that the corrosion resistance of the TZAM8110 alloy can be greatly improved by utilizing the PEB treatment.

The SEM micrographs in Figs. 8 and 9 show the microstructural changes occurring in the surface areas of the as-extruded and PEB-treated samples, respectively, during immersion in 0.6 M NaCl solution. Dissolution of α-Mg around Mg_2Sn particles can be seen in the as-extruded sample after immersion for 0.5 h, revealing the occurrence of microgalvanic corrosion at the early stage of immersion. After immersion for 1 h, the as-extruded sample became more deeply corroded, exhibiting the formation of cracked oxides, while the modified surface layer of the PEB-treated sample was not seriously attacked by corrosion. After immersion for 4 h, the as-extruded sample showed a more seriously corroded surface, mostly being covered with oxides, whereas only a part of the modified surface layer was damaged by corrosion in the PEB-

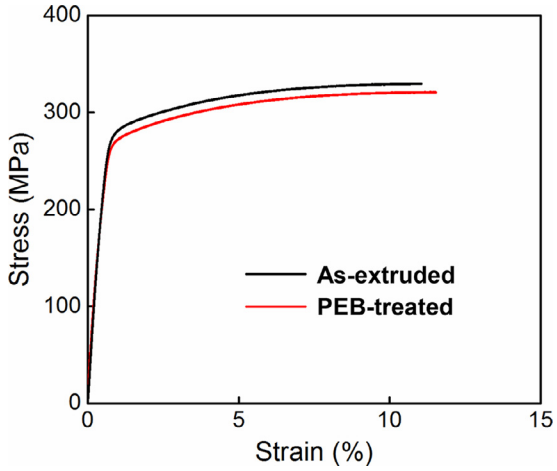

Fig. 6. Tensile stress-strain curves of the as-extruded and PEB-treated samples.

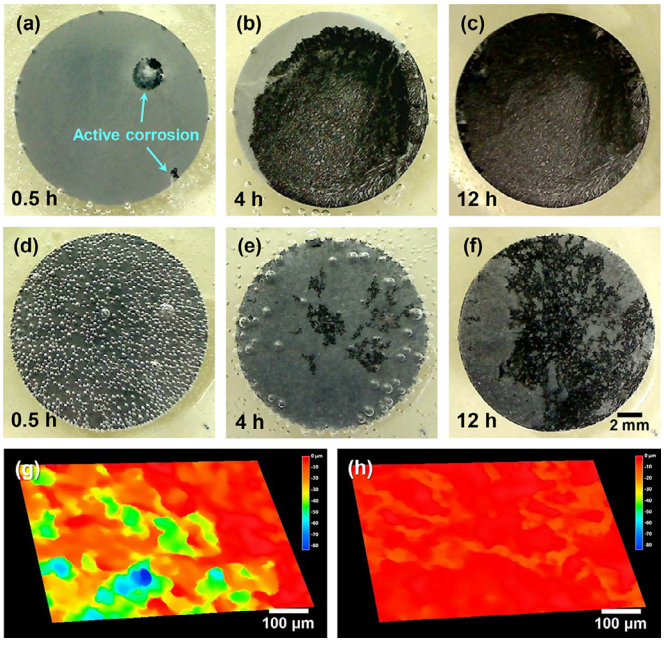

Fig. 7. Optical micrographs of the (a-c) as-extruded and (d-f) PEB-treated samples after immersion for 0.5~12 h in 0.6 M NaCl solution and depth profiles showing the surface roughness of the (g) as-extruded and (h) PEB-treated samples after immersion in 0.6 M NaCl solution for 12 h. The sample surfaces are perpendicular to the ED.

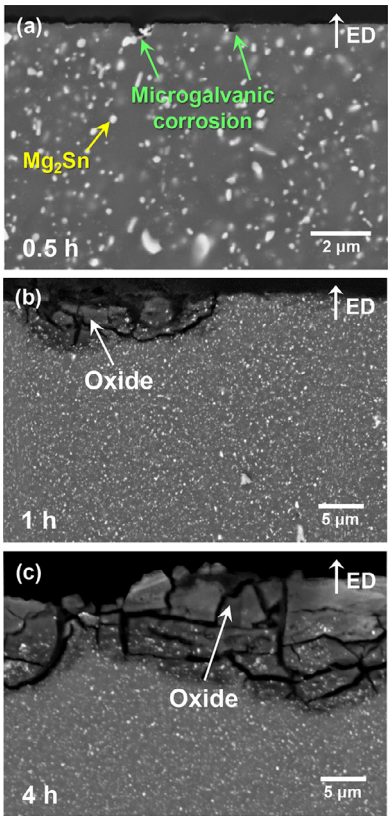

Fig. 8. SEM micrographs showing cross-sections of the as-extruded sample after immersion in 0.6 M NaCl solution for (a) 0.5 h, (b) 1 h, and (c) 4 h.

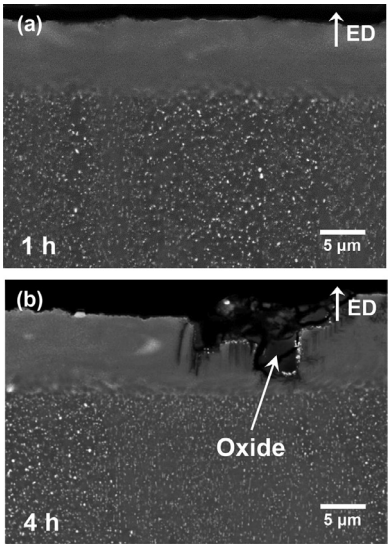

Fig. 9. SEM micrographs showing cross-sections of the PEB-treated sample after immersion in 0.6 M NaCl solution for (a) 1 h and (b) 4 h.

treated sample. Here, it is interesting that the modified surface layer of the PEB-treated sample did not completely disappear after immersion for 4 h even in the highly damaged area. This indicates that the modified surface layer of the PEB-treated sample affords greater protection than the bare surface of the as-extruded alloy.

Fig. 10a shows the collected H_2 volume values of the as-extruded and PEB-treated samples during immersion for up to 72 h in 0.6 M NaCl solution. As expected, it was found that the PEB-treated sample generates a relatively smaller amount of H_2 than that of the as-extruded sample. The amounts of collected H_2 volume after immersion for 72 h were 5.8±0.4 and 2.8±0.2 ml cm^{-2} for the as-extruded and PEB-treated samples, respectively. As indicated in Fig. 10b, the weight loss values obtained after immersion for 72 h were 12.0±0.3 and 6.5±0.3 mg cm^{-2} for the as-extruded and PEB-treated samples, respectively, which correspond to corrosion rates of 8.1±0.2 and 4.3±0.2 mm y^{-1}, respectively.

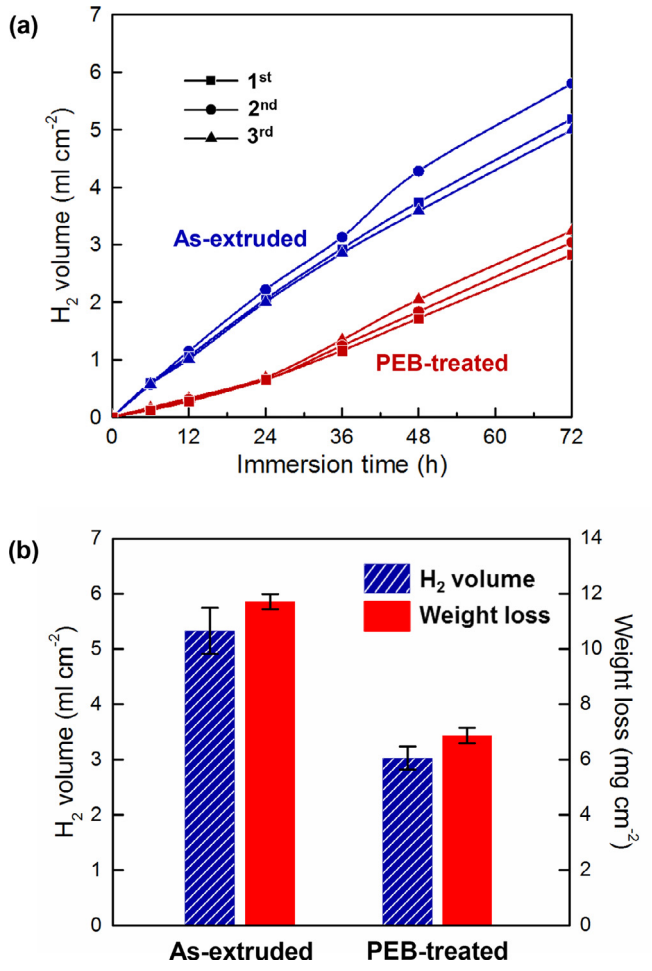

Fig. 10. (a) Collected H_2 volume values of the as-extruded and PEB-treated samples as a function of immersion time and (b) H_2 volume and weight loss values of the as-extruded and PEB-treated samples after immersion for 72 h in 0.6 M NaCl solution.

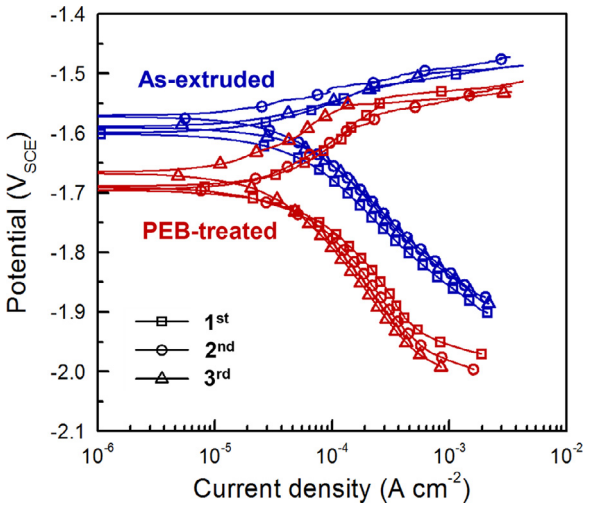

Fig. 11. Potentiodynamic polarization curves of the as-extruded and PEB-treated samples in 0.6 M NaCl solution.

The potentiodynamic polarization curves of the as-extruded and PEB-treated samples in 0.6 M NaCl solution are presented in Fig. 11. First, the corrosion potential (E_{corr}) of the PEB-treated sample was found to be lower than that of the as-extruded sample; the E_{corr} values of the as-extruded and PEB-treated samples are -1.59 ± 0.01 and -1.68 ± 0.02 V_{SCE}, respectively. The cathodic branch of the curves indicates that the PEB-treated sample has a cathodic current density ($i_{cathodic}$) that is much lower than that of the as-extruded sample. For instance, the $i_{cathodic}$ values measured at -1.80 V_{SCE} were -0.54 ± 0.09 and -0.13 ± 0.03 mA cm^{-2} for the as-extruded and PEB-treated samples, respectively. The anodic branch of the curves shows that the passive current density value of the PEB-treated sample is somewhat higher than that of the as-extruded sample, indicating that the PEB treatment degrades passivity. From the polarization curves, values of a cathodic Tafel slope ($ß_c$) and a corrosion current density (i_{corr}) were measured following methods in the literature [37,38]. The $ß_c$ values were found to be -175 ± 6 and -262 ± 20 mV decade^{-1} and the i_{corr} values were found to be -37.4 ± 2.5 and -30.0 ± 2.7 μA cm^{-2} for the as-extruded and PEB-treated samples, respectively.

3.3. Corrosion-controlling factor

The present study shows that the corrosion resistance of the extruded TZAM8110 alloy can be considerably improved by surface modification using the PEB treatment. Prior to the PEB treatment, the alloy revealed a microstructure containing Mg_2Sn precipitates with sizes of 0.1∼1 μm, which can act as microscale cathodes due to their electrochemically noble character relative to α-Mg. To lessen the role of the noble cathodic particles in activating corrosion, the PEB treatment was applied to a Mg_2Sn-dispersed alloy, and the PEB treatment was found to be an effective way of selectively eliminating the pre-existing Mg_2Sn precipitates in the alloy. Experimental observations showed that the modified surface layer formed by the PEB treatment is more resistant to degradation in a corrosive environment than the original surface of the alloy without the PEB treatment. This clearly demonstrates that the PEB-induced surface modification toward reducing the Mg_2Sn precipitates has a beneficial effect on the corrosion resistance of the TZAM8110 alloy, which is consistent with a decrease in $i_{cathodic}$ after the PEB treatment in the cathodic branch of the polarization curves.

This change in the presence of Mg_2Sn precipitates on the surface is necessarily accompanied by an increase in the Sn content solutionized in the α-Mg matrix. It must be considered because the increased Sn content within the α-Mg matrix can accelerate the anodic reaction rate during corrosion, as previously reported [21,39]. The case in this study is considered to be different from the previously reported PEB-treated AZ91 alloy in that an increase in the Al content due to dissolution of the Al-containing particles can contribute to a decrease in the anodic reaction rate [26,39]. In this regard, the corrosion-related results of the TZAM8110 alloys with and without the PEB treatment cannot be properly interpreted

when only considering the abovementioned role of alloyed Sn in the acceleration of the anodic reaction rate. One more aspect to consider here is that the passive film formed on Mg alloys generally does not have sufficient protectiveness, being different from that of Ti or Al alloys [29,31], and it is thus capable of protecting the alloys merely at an early stage of immersion prior to the occurrence of severe localized corrosion. This suggests that a factor affecting anodic activation might not be critically responsible for the long-term corrosion behavior of Mg alloys, which typically exhibit limited passivity. In this regard, the PEB-induced improvement in the corrosion resistance is thought to be primarily ascribable to the reduction of the noble Mg_2Sn precipitates on the surface, such that their role in cathodic activation during corrosion is diminished.

4. Conclusion

The effect of the PEB treatment on the microstructure and corrosion properties of extruded TZAM8110 alloy containing Mg_2Sn precipitates was investigated. It was found that the pre-existing precipitates were selectively removed after the PEB treatment, forming a modified surface layer with reduced precipitates. Microstructural observations indicated that the modified surface layer is more resistant to corrosion-induced degradation than the bare alloy without the PEB treatment. The average corrosion rates, evaluated by immersion tests in 0.6 M NaCl solution at 25 °C, were 8.1 and 4.3 mm y^{-1} for the as-extruded and PEB-treated samples, respectively. The improvement in the corrosion resistance attained by surface modification through the PEB treatment is attributed to the reduction of noble Mg_2Sn precipitates, which in turn would diminish their role in cathodic activation in the corrosive condition.

Acknowledgement

This work was supported by the National Research Foundation of Korea (NRF) grant funded by the Korea government (MSIT) (No. 2019R1A2C1003905).

References

[1] N.J. Kim, Mater. Sci. Technol. 30 (2014) 1925–1928.
[2] T.T. Sasaki, K. Yamamoto, T. Honma, S. Kamado, K. Hono, Scr. Mater. 59 (2008) 1111–1114.
[3] D.H. Kang, D.-W. Kim, S. Kim, G.T. Bae, K.H. Kim, N.J. Kim, Scr. Mater. 61 (2009) 768–771.
[4] W.L. Cheng, S.S. Park, B.S. You, B.H. Koo, Mater. Sci. Eng. A 527 (2010) 4650–4653.
[5] S.S. Park, B.S. You, Scr. Mater. 65 (2011) 202–205.
[6] H.Y. Jeong, B. Kim, S.-G. Kim, H.J. Kim, S.S. Park, Mater. Sci. Eng. A 612 (2014) 217–222.
[7] M. Yuasa, N. Miyazawa, M. Hayashi, M. Mabuchi, Y. Chino, Acta Mater. 83 (2015) 294–303.
[8] T.T. Sasaki, F.R. Elsayed, T. Nakata, T. Ohkubo, S. Kamado, K. Hono, Acta Mater. 99 (2015) 176–186.
[9] B.-C. Suh, J.H. Kim, J.H. Hwang, M.-S. Shim, N.J. Kim, Sci. Rep. 6 (2016) 22364.
[10] B.-C. Suh, J.H. Kim, J.H. Bae, J.H. Hwang, M.-S. Shim, N.J. Kim, Acta Mater. 124 (2017) 268–279.
[11] T.T.T. Trang, J.H. Zhang, J.H. Kim, A. Zargaran, J.H. Hwang, B.-C. Suh, N.J. Kim, Nat. Commun. 9 (2018) 2522.
[12] M.Z. Bian, T.T. Sasaki, B.-C. Suh, T. Nakata, S. Kamado, K. Hono, Scr. Mater. 138 (2017) 151–155.
[13] D.H. Kang, S.S. Park, N.J. Kim, Mater. Sci. Eng. A 413–414 (2005) 555–560.
[14] T.T. Sasaki, K. Oh-ishi, T. Ohkubo, K. Hono, Scr. Mater. 55 (2006) 251–254.
[15] D.H. Kang, S.S. Park, Y.S. Oh, N.J. Kim, Mater. Sci. Eng. A 449–451 (2007) 318–321.
[16] S. Wei, Y. Chen, Y. Tang, H. Liu, S. Xiao, G. Niu, X. Zhang, Y. Zhao, Mater. Sci. Eng. A 492 (2008) 20–23.
[17] M.A. Gibson, X. Fang, C.J. Bettles, C.R. Hutchinson, Scr. Mater. 63 (2010) 899–902.
[18] S.H. Park, S.-H. Kim, H.S. Kim, J. Yoon, B.S. You, J. Alloy. Compd. 667 (2016) 170–177.
[19] J. Yoon, S.H. Park, Mater. Des. 55 (2014) 300–308.
[20] A. Pardo, M.C. Merino, A.E. Coy, F. Viejo, R. Arrabal, S. Feliu Jr., Electrochim. Acta 53 (2008) 7890–7902.
[21] H.-Y. Ha, J.-Y. Kang, S.G. Kim, B. Kim, S.S. Park, C.D. Yim, B.S. You, Corros. Sci. 82 (2014) 369–379.
[22] H.J. Kim, B. Kim, S.-M. Baek, S.-D. Sohn, H.-J. Shin, H.-Y. Jeong, C.D. Yim, B.S. You, H.-Y. Ha, S.S. Park, Corros. Sci. 95 (2015) 133–142.
[23] H.-Y. Ha, H.J. Kim, S.-M. Baek, B. Kim, S.-D. Sohn, H.-J. Shin, H.Y. Jeong, S.H. Park, C.D. Yim, B.S. You, J.G. Lee, S.S. Park, Scr. Mater. 109 (2015) 38–43.
[24] S.-M. Baek, H.J. Kim, H.Y. Jeong, S.-D. Sohn, H.-J. Shin, K.-J. Choi, K.-S. Lee, J.G. Lee, C.D. Yim, B.S. You, H.-Y. Ha, S.S. Park, Corros. Sci. 112 (2016) 44–53.
[25] X. Liu, D. Shan, Y. Song, R. Chen, E. Han, Electrochim. Acta 56 (2011) 2582–2590.
[26] B. Gao, S. Hao, J. Zou, W. Wu, G. Tu, C. Dong, Surf. Coat. Technol. 201 (2007) 6297–6303.
[27] S. Hao, X. Zhang, X. Mei, T. Grosdidier, C. Dong, Mater. Lett. 62 (2008) 414–417.
[28] J. Kim, S.S. Park, H.W. Park, Corros. Sci. 89 (2014) 179–188.
[29] X.D. Zhang, S.Z. Hao, Li X.N, C. Dong, T. Grosdidier, Appl. Surf. Sci. 257 (2011) 5899–5902.
[30] Y. Samih, G. Marcos, N. Stein, N. Allain, E. Fleury, C. Dong, T. Grosdidier, Surf. Coat. Technol. 259 (2014) 737–745.
[31] J. Kim, H.W. Park, Corros. Sci. 90 (2015) 153–160.
[32] Y.R. Liu, K.M. Zhang, J.X. Zou, D.K. Liu, T.C. Zhang, J. Alloy. Compd. 741 (2018) 65–75.
[33] G. Song, A. Atrens, Adv. Eng. Mater. 5 (2003) 837–858.
[34] A.E. Coy, F. Viejo, P. Skeldon, G.E. Thompson, Corros. Sci. 52 (2010) 3896–3906.
[35] A. Atrens, G.-L. Song, M. Liu, Z. Shi, F. Cao, M.S. Dargusch, Adv. Eng. Mater. 17 (2015) 400–453.
[36] M. Esmaily, J.E. Svensson, S. Fajardo, N. Birbilis, G.S. Frankel, S. Virtanen, R. Arrabal, S. Thomas, L.G. Johansson, Prog. Mater. Sci. 89 (2017) 92–193.
[37] M. Liu, P. Schmutz, P.J. Uggowitzer, G. Song, A. Atrens, Corros. Sci. 52 (2010) 3687–3701.
[38] A.D. Sudholz, K. Gusieva, X.B. Chen, B.C. Muddle, M.A. Gibson, N. Birbilis, Corros. Sci. 53 (2011) 2277–2282.
[39] K. Gusieva, C.H.J. Davies, J.R. Scully, N. Birbilis, Int. Mater. Rev. 60 (2015) 169–194.